Mega-xenocrysts in alkali olivine basalts: Fragments of disrupted mantle assemblages

Kevin Righter, Ian S. E. Carmichael

Department of Geology and Geophysics, University of California, Berkeley, California 94720, U.S.A.

Abstract

Megacrysts of augite (34), feldspar (12), kaersutite (10), olivine (8), and biotite (1) from eight alkali basalt localities in the western U.S. and Mexico have been analyzed by electron microprobe and wet chemical techniques. These crystals range from 1 to 10 cm, are free of inclusions, and are unzoned. Such crystals cannot have grown from the basalt host, as that would require unreasonably large growth and diffusion rates. In addition, many of the megacrysts have fragmented or irregular edges in contact with the host basalt. With these constraints, such unzoned megacrysts must be xenocrysts acquired along the ascent path of the basalt host. Their composition and large size indicate that many of the megacrysts could be derived from disaggregated gabbroic (olivine, augite, plagioclase, kaersutite, biotite), pyroxenitic (augite), wehrlitic (olivine and augite), and syenitic (anorthoclase) dikes or pegmatites.

Introduction

Megacrysts of clinopyroxene, orthopyroxene, amphibole, feldspar, phlogopite, oxide, and olivine are found in alkali basalt at many localities throughout the world. These megacrysts are typically 1–10 cm in size, are compositionally homogeneous, and may have a glassy appearance. It is commonly stated in the literature that these megacrysts are high-pressure cognate near-liquidus phases (Irving, 1974; Irving and Frey, 1984; Wilkinson and LeMaitre, 1987). Major element partitioning and isotopic data are "consistent with an equilibrium relationship" between augite and host at high pressures (Irving and Frey, 1984) but are certainly not demonstrative of equilibrium. Similarly, as one of the many explanations for the origin of kaersutite megacrysts in alkali basalts, Wilkinson and LeMaitre (1987) stated that an equilibrium relationship between kaersutite megacrysts and host lavas at high pressures "would receive the widest support." There is, however, evidence at many localities for disequilibrium between kaersutite and its host lavas (Stuckless and Irving, 1976; Basu, 1978; Bergman and Foland, 1981; Foland et al., 1983). From the data reported and discussed in the literature, it is not clear that any of the megacrysts can be shown to be in equilibrium with their host lavas. The relation between megacryst suites and associated Group I (chromian diopside) and Group II (aluminous augite) mantle xenoliths is also unclear (Wilshire and Shervais, 1975; Frey and Prinz, 1978).

The compositionally unzoned nature of the megacrysts requires many to have crystallized slowly, either in a magma chamber or in dikes or pegmatites within the crust or mantle. The goal of this study is to determine if any of the megacrysts crystallized from magmas similar to their basaltic hosts, or if they represent disaggregated pieces of mantle peridotite or pyroxenite. We have collected augite, kaersutite, feldspar, biotite, and olivine megacrysts and host basalt from eight localities in the western U.S. and Mexico (Fig. 1, Appendix 1). Megacryst and gabbroic xenolith minerals were analyzed by electron microprobe and the host lavas by X-ray fluorescence spectroscopy (Tables 1–6, Appendix 2). Fe^{2+} in the host lavas and in the augite and kaersutite megacrysts was determined by wet chemical techniques. Using petrographic information, major element microprobe traverses, augite redox equilibria, minor- and trace-element partitioning relations, and isotopic data from the literature it can be demonstrated that many megacrysts could be in compositional, but not textural, equilibrium with their hosts at pressures of 5–15 kbar. Megacrysts that appear to be in compositional equilibrium with their host may have been derived from disaggregated gabbroic or pyroxenitic cumulates, veins, or pegmatites.

Megacrysts: Size, zoning, and growth rates

The most intriguing aspects of megacrysts are their large size and their lack of either compositional zoning or mineral and glass inclusions. Augite samples up to 70 mm have been described from the Dish Hill and Lunar Crater localities (Wilshire et al., 1988), as have olivines as large as 50×50 mm from Lunar Crater, feldspars up to 30 mm from Cima Volcanic Field, and kaersutite samples up to 30–40 mm from the Dish Hill and Cima localities (Wilshire et al., 1988). Previous studies (Binns et al., 1970; Irving, 1974; Aoki, 1970) have reported the compositional homogeneity of many megacryst phases; this is illustrated for an augite sample and a kaersutite sample from Lunar Crater and a feldspar from Valle de Santiago (Fig. 2). Compositional homogeneity of the feldspars, represented by the standard deviation σ_{An} is recorded in Table 3. With the exception of kaersutite, megacrysts are
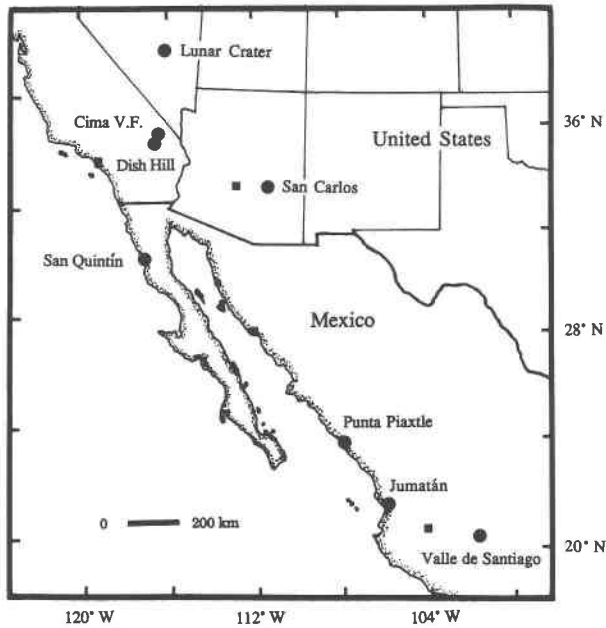
Fig. 1. Location map for the samples analyzed for this study (circles). Major cities from north to south are Los Angeles, Phoenix, Guaymas, and Guadalajara (squares). Brief descriptions and references for each locality are given in Appendix 1.

inclusion-free (augite, olivines, and feldspars). In some kaersutite megacrysts there are inclusions of sulfide (at San Carlos) and exsolution of pseudobrookite (at Lunar Crater).

A hypothesis advanced by Carmichael et al. (1977) is that megacrysts precipitated at high pressures in thermal response to cooler, engulfed xenolith nodules. This hypothesis has several drawbacks. First, augite from most localities (Jumatán, Valle de Santiago, San Quintín, Cima, Dish Hill, Lunar Crater) has broken or fragmented edges. That from Punta Piaxtle is rounded and fractured. Both of these textural characteristics are not consistent with

growth from the host. Second, this hypothesis is inconsistent with the required growth rates. Precipitation at high pressures would require rapid growth of megacrysts, at large degrees of undercooling (ΔT) in order to avoid compositional zoning, which may occur when P and T change upon ascent. If a change in pressure of 1 kbar (~ 3 km) is the minimum to cause detectable (by microprobe) megacryst compositional change, the time taken to traverse this distance (upon ascent) would be approximately 6×10^3 s (with an ascent rate of 50 cm/s: Spera, 1984). For megacrysts to attain a length of 4 cm (2-cm radius) thus requires a growth rate of at least 3.3×10^{-4} cm/s. Such growth rates have been attained experimentally for fassaite (Lofgren, 1990) and diopside and anorthite (Kirkpatrick et al., 1976), in melts of their own composition. Similar experiments (large ΔT) on natural lavas resulted in skeletal and dendritic crystal textures (Kirkpatrick, 1975; Walker et al., 1976; Grove, 1978), in stark contrast to the universally glass-inclusion-free megacrysts. For these reasons, it seems unlikely that megacrysts grew rapidly; it is likely it grew slowly, in a magma chamber, vein, or pegmatite.

Megacrysts may have precipitated from their host magmas and grown slowly, without compositional zoning, at low growth rates of 10^{-10}–10^{-11} cm/s (plagioclase, augite, olivine: Cashman and Marsh, 1988; Marsh et al., 1991); it would require thousands of years to grow 1-cm crystals. Growth rates for unzoned megacrysts may be even lower, as the above rates were determined from slightly zoned phenocrysts in lava lakes and laccoliths. The above growth rates are therefore an upper limit on growth rates appropriate for megacrysts. Variables such as temperature, pressure, and f_{O_2} would have to remain relatively constant during this time period (thousands of years) to ensure the growth of compositionally homogeneous crystals. Such conditions may prevail in a long-lived magma chamber. Volcanism began 9 Ma at Cima Volcanic Field (Wilshire et al., 1991) and 7 Ma at Lunar Crater Volcanic Field (Bergman, 1982) and continues to the present at
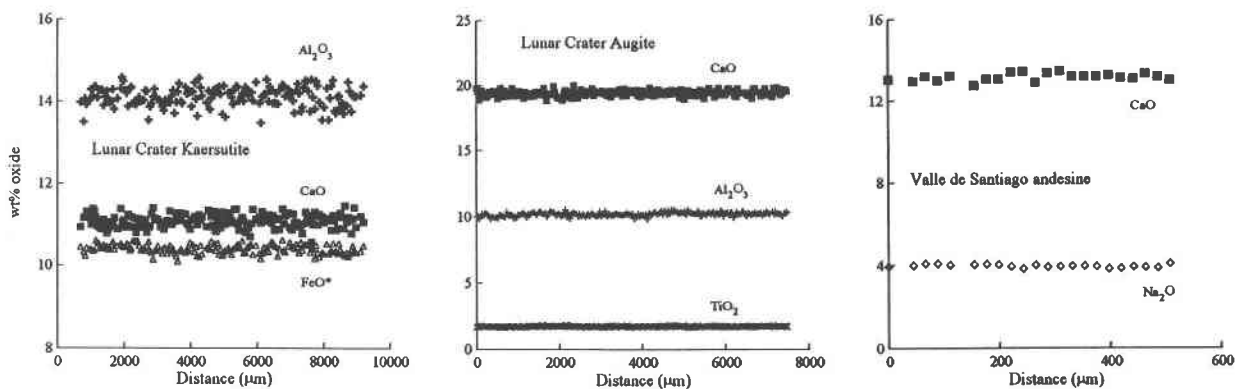

Fig. 2. Electron microprobe analyses across a 7.5-mm augite megacryst and a 1-cm kaersutite megacryst, both from the Lunar Crater Volcanic Field, and 0.4 mm of a larger (1.5 cm) feldspar megacryst from the Valle de Santiago area. Note the lack of compositional zoning across the entire length of the traverses.

TABLE 1. Augite megacryst analyses

Oxide	Lunar Crater augite						Cima V.F.		Dish Hill			
	1	2	3	4	5	6	1	2	1	2	3	4
SiO_2	49.9	48.6	48.9	47.2	47.1	48.8	46.9	48.2	47.7	48.9	47.8	48.3
TiO_2	0.86	1.21	1.00	1.75	1.80	1.04	1.89	1.35	1.86	1.26	1.81	1.87
Al_2O_3	8.3	9.4	8.8	10.3	10.7	10.2	9.7	9.1	9.4	9.2	9.0	8.9
Cr_2O_3	0.24	0.01	0.14	0.11	0.03	0.03	0.00	0.01	0.01	0.01	0.01	0.01
Fe_2O_3	2.14	2.37	2.20	3.93	2.94	2.03	3.85	2.40	2.98	2.55	3.28	3.17
FeO	3.22	3.9	3.36	3.45	4.35	3.74	4.54	4.15	4.38	4.01	4.58	4.57
MnO	0.14	0.16	0.11	0.17	0.27	0.22	0.11	0.11	0.27	0.29	0.32	0.32
NiO	0.03	0.02	0.01	0.00	0.00	0.00	0.00	0.00	0.01	0.01	0.01	0.01
MgO	15.4	14.2	14.3	12.7	12.9	14.7	12.7	13.6	12.8	13.8	12.9	12.7
CaO	19.23	19.38	19.6	19.58	19.56	19.52	19.22	19.92	19.19	18.76	19.01	19.11
Na_2O	0.91	0.99	0.92	1.22	1.23	0.99	0.99	0.73	1.11	0.98	1.12	1.10
Total	100.39	100.20	99.29	100.44	100.80	101.22	99.91	99.55	99.75	99.83	99.79	100.06
FeO_{tot}	5.14	6.03	5.34	6.99	7.00	5.57	8.01	6.31	7.06	6.30	7.53	7.43
R	0.38	0.37	0.38	0.50	0.38	0.35	0.44	0.35	0.36	0.37	0.39	0.39
Fe^{3+}/Fe^{2+}	0.60	0.55	0.59	1.03	0.61	0.49	0.76	0.52	0.61	0.57	0.64	0.63
Mg' (molar)	0.90	0.87	0.90	0.87	0.84	0.87	0.83	0.85	0.84	0.86	0.83	0.83
Mg' (wt)	0.83	0.78	0.82	0.79	0.75	0.80	0.74	0.77	0.74	0.78	0.74	0.73

Oxide	Dish Hill augite			San Carlos augite						San Quintín	
	5	6	7	1	2	3	4	5	6	78	82
SiO_2	48.2	47.9	47.9	47.3	47.9	47.6	47.5	47.7	49.1	48.7	48.6
TiO_2	1.88	1.89	1.82	1.88	1.58	1.87	1.87	1.74	0.79	1.50	1.41
Al_2O_3	9.0	9.2	8.9	9.9	9.8	9.9	9.9	9.9	5.8	8.8	9.2
Cr_2O_3	0.00	0.01	0.00	0.01	0.01	0.01	0.01	0.01	0.01	0.03	0.04
Fe_2O_3	3.05	3.19	3.23	3.08	2.90	3.16	3.28	3.11	4.65	2.46	3.08
FeO	4.64	4.79	4.60	5.40	5.20	5.28	5.17	5.01	9.27	6.54	5.75
MnO	0.31	0.29	0.30	0.33	0.35	0.33	0.33	0.34	0.59	0.17	0.18
NiO	0.00	0.01	0.00	0.01	0.01	0.00	0.01	0.01	0.01	0.00	0.00
MgO	13.0	12.8	12.8	12.3	13.1	12.5	12.6	12.8	8.7	14.1	14.0
CaO	19.04	18.87	19.07	17.90	17.82	18.10	18.16	18.23	19.29	17.00	17.22
Na_2O	1.09	1.11	1.13	1.46	1.40	1.46	1.44	1.40	1.98	1.19	1.06
Total	100.21	100.06	99.75	99.56	100.04	100.23	100.19	100.19	100.14	100.49	100.52
FeO_{tot}	7.38	7.66	7.51	8.17	7.81	8.12	8.12	7.81	13.45	8.76	8.52
R	0.39	0.38	0.39	0.35	0.33	0.36	0.36	0.38	0.31	0.26	0.32
Fe^{3+}/Fe^{2+}	0.59	0.60	0.63	0.51	0.50	0.54	0.57	0.56	0.45	0.34	0.48
Mg' (molar)	0.83	0.83	0.83	0.80	0.82	0.81	0.81	0.82	0.63	0.79	0.82
Mg' (wt)	0.74	0.73	0.74	0.70	0.72	0.70	0.71	0.72	0.48	0.68	0.71

Oxide	Valle de Santiago				Jumatán		Punta Piaxtle				
	229	152	211	104	Black	Green	PR-1	PX-1	PX-3	PX-4	PX-5
SiO_2	48.5	47.7	46.9	48.3	49.5	51.5	47.7	48.1	50.7	47.5	48.4
TiO_2	1.62	2.25	2.16	2.13	1.02	0.46	1.28	1.17	0.43	1.35	1.12
Al_2O_3	8.6	8.0	8.6	7.4	6.9	5.2	9.8	9.7	7.3	9.8	9.6
Cr_2O_3	0.14	0.01	0.01	0.07	0.03	0.77	0.01	0.01	1.10	0.01	0.01
Fe_2O_3	1.95	3.46	3.12	3.19	1.96	0.42	2.62	2.81	1.12	2.16	2.38
FeO	5.61	5.60	6.32	6.02	3.89	3.21	5.14	4.30	3.14	5.70	4.54
MnO	0.13	0.11	0.14	0.10	0.03	0.08	0.16	0.15	0.11	0.17	0.14
NiO	0.00	0.00	0.01	0.00	0.00	0.00	0.01	0.02	0.06	0.02	0.03
MgO	14.0	12.7	12.9	13.2	14.7	16.7	13.5	13.9	16.9	13.3	13.9
CaO	19.08	19.56	19.70	19.84	21.31	20.95	19.07	19.38	18.85	19.18	19.26
Na_2O	0.76	0.96	0.85	0.86	0.46	0.42	0.80	0.77	0.59	0.77	0.79
Total	100.39	100.39	100.61	101.06	99.77	99.64	100.09	100.31	100.30	99.96	100.1
FeO_{tot}	7.36	8.72	9.13	8.89	5.66	3.59	7.50	6.83	4.15	7.64	6.68
R	0.23	0.37	0.31	0.33	0.31	0.11	0.31	0.37	0.24	0.25	0.32
Fe^{3+}/Fe^{2+}	0.31	0.56	0.44	0.48	0.45	0.12	0.46	0.59	0.32	0.34	0.47
Mg' (molar)	0.82	0.80	0.78	0.80	0.87	0.90	0.82	0.85	0.91	0.81	0.85
Mg' (wt)	0.71	0.69	0.67	0.69	0.79	0.84	0.72	0.76	0.84	0.70	0.75

both localities, indicating that long-lived magma chambers exist beneath these areas. Even if megacrysts have grown slowly from an alkali basalt melt, they cannot be phenocrysts, as many are either rounded or have broken, fragmented edges. Only augite samples from San Carlos have shapes that are subhedral, and these are only on one side of a megacryst. Given these textural characteristics, megacrysts must represent disaggregated pegmatites, veins, or cumulates, derived upon ascent.

Megacrysts lack reaction rims, which one might expect

TABLE 2. Amphibole and mica megacryst analyses

Oxide	San Carlos amphibole					Lunar Crater amphibole						Psb 5*	Valle de Santiago GM-103
	1	3	4	5	Mica	1	2	3	4	5	6		
SiO_2	39.2	39.2	39.5	39.2	33.8	39.4	39.5	39.5	39.3	39.2	39.1	0.2	40.8
TiO_2	5.02	4.86	5.06	5.70	7.40	6.50	5.54	6.19	6.11	6.07	6.17	54.70	3.28
Al_2O_3	13.2	13.2	14.0	13.8	14.6	15.0	15.0	14.8	14.7	14.7	14.7	0.5	13.0
Cr_2O_3	0.01	0.02	0.00	0.00	0.00	0.01	0.02	0.02	0.02	0.01	0.01	—	—
Fe_2O_3	9.08	4.90	9.99	3.04	2.60	7.68	4.81	9.35	7.44	2.92	3.68	34.66	5.99
FeO	8.52	12.42	5.99	10.30	17.30	4.02	6.43	2.67	4.11	7.83	7.49	1.80	6.68
MnO	0.42	0.41	0.32	0.31	0.34	0.13	0.11	0.12	0.28	0.30	0.31	—	0.14
NiO	0.00	0.00	0.00	0.00	0.00	0.01	0.01	0.02	0.00	0.00	0.00	—	0.00
ZnO	0.00	0.00	0.00	0.00	0.00	0.02	0.02	0.01	0.00	0.00	0.00	—	0.00
MgO	8.4	9.3	10.2	11.0	8.7	11.4	11.1	11.4	12.7	12.8	12.8	8.3	12.7
CaO	10.29	10.32	9.93	9.98	0.01	10.95	11.28	10.96	11.14	11.30	11.21	0.41	11.12
Na_2O	2.19	2.27	3.21	2.86	0.66	2.62	2.72	2.65	2.53	2.42	2.56	—	2.67
K_2O	2.10	2.06	1.29	1.31	8.98	1.17	1.09	1.16	1.26	1.24	1.20	—	0.57
F^-	0.08	0.08	0.08	0.07	0.10	0.00	0.00	0.00	0.04	0.06	0.07	—	0.12
Total	98.43	99.05	99.65	97.67	94.49	98.89	97.62	98.84	99.57	98.91	99.26	100.58	96.51
FeO_{tot}	16.69	16.83	14.98	13.04	19.64	10.93	10.76	11.08	10.81	10.46	10.80	32.96	12.07
R	0.49	0.26	0.60	0.21	0.12	0.63	0.40	0.76	0.62	0.25	0.31		0.45
Fe^{3+}/Fe^{2+}	0.96	0.36	1.50	0.27	0.14	1.72	0.67	3.15	1.63	0.34	0.44	—	0.81
Mg' (molar)	0.64	0.57	0.75	0.66	0.47	0.83	0.75	0.88	0.85	0.74	0.75	—	0.77
Mg' (wt)	0.50	0.43	0.63	0.52	0.33	0.74	0.63	0.81	0.76	0.62	0.63	—	0.66

* Fe_2O_3 for pseudobrookite calculated using charge balance and stoichiometry considerations.

of minerals that are not in equilibrium with their host lavas. The experiments of Tsuchiyama (1986) demonstrated that olivine xenocrysts do not develop pyroxene reaction rims when pyroxene is not on the liquidus of the host liquid. Since orthopyroxene is not a phenocryst in any of these host lavas, it is not surprising that the olivines do not have reaction rims. These minerals also lack compositional zoning, which may form as a xenocryst starts to reequilibrate with its host. A magma ascending from 50 km (~15 kbar) at an ascent rate of 50 cm/s (Spera, 1984), requires approximately 30 h to reach the surface. Thus, any diffusion-controlled compositional zoning in a xenocryst must occur within this time frame. Mg-Fe diffusion rates in olivine are the fastest of any megacryst phase in this study, and these require ~1600 yr to homogenize a 1-cm Fo_{90} crystal (Buenig and Buseck, 1973). It is clear that originally unzoned xenocrysts may remain unzoned after incorporation into the magma; diffusion-controlled zoning will not develop on such a short time scale as the ascent time of these magmas.

MEGACRYST SOURCES: XENOLITHS

It is clear from textural observations (fragmented or rounded megacrysts, without zoning) that these megacrysts must be xenocrysts, derived from along the ascent path of the alkali basalt magma. The question remains, however, from what rock type are the megacrysts derived? Mantle peridotites and pyroxenites, both Type I (chromian diopside) and Type II (aluminous augite), and gabbroic xenoliths are found at most localities.

Gabbroic and pyroxenitic xenoliths

Gabbroic and pyroxenitic xenoliths are found at many of the megacryst localities (see Appendix 1 and Wilshire

et al., 1988), evidence that crystal accumulation has occurred under these areas. These gabbros contain olivine, augite, plagioclase, kaersutite, and Fe-Ti oxides (see Table 6 for Valle de Santiago and Jumatán mineral data). In fact, oceanic island localities (Hawaii: Fodor and Vandermeyden, 1988; Reunion: Upton and Wadsworth, 1972; Galapagos: McBirney and Williams, 1969; Gough: LeMaitre, 1965) and continental localities (New South Wales: Wilshire and Binns, 1961) both have gabbroic xenoliths containing aluminous augite, and such rocks also occur in layered intrusions (Kiglapait: Morse, 1980; Newark Island: Wiebe and Snyder, 1993; Cumberland: Rutherford and Hermes, 1984). The assemblage olivine + augite + magnetite + ilmenite allows one to calculate P, if the composition of each of these phases is known (Frost and Lindsley, 1992). We have applied Ca-QUIIF equilibria (Lindsley and Frost, 1992) to 15 gabbro samples from the above localities in order to estimate pressure. Gabbros that equilibrated at higher pressures (~15 kbar) generally have more sodic feldspars (Fig. 3) and aluminous augite. It is clear that the megacrysts could originate in a gabbroic rock, and thus at pressures of 5–15 kbar. Could the gabbros and pyroxenites have crystallized from the host magmas that brought them to the surface? Equilibrium crystallization calculations at 10 kbar, with a regular solution model for silicate liquids (SILMIN: Ghiorso et al., 1983), predict mineral compositions that are nearly identical to those measured in gabbro xenoliths at the Cima, San Carlos, Jumatán, and Valle de Santiago localities (Table 7).

Hydrous veins and pegmatites

Many composite peridotite xenoliths and peridotite massifs contain veins or pegmatites of pyroxenite, am-

TABLE 3. Feldspar megacryst analyses

Oxide	Lunar Crater	Cima V.F.		San Carlos			San Quintín		Punta Piaxtle	Jumatán			Valle de Santiago	
	1	1	2	1	2	3	77	81	PX-2	1	2	3	152	14
SiO_2	61.0	65.7	66.0	64.8	64.0	64.7	60.2	59.2	55.6	47.3	46.8	54.2	52.3	55.5
Al_2O_3	23.9	20.3	19.9	20.7	21.6	20.7	25.2	25.8	28.0	34.0	34.0	28.7	29.6	28.6
FeO	0.20	0.17	0.17	0.16	0.17	0.16	0.21	0.22	0.29	0.31	0.36	0.36	0.33	0.33
CaO	4.39	1.06	0.69	1.26	2.18	1.43	5.98	6.87	10.24	16.61	16.82	10.42	11.82	9.84
Na_2O	8.32	7.73	7.14	7.25	7.89	7.92	7.71	7.51	5.48	1.90	1.58	5.61	4.67	5.74
K_2O	1.34	5.34	6.65	5.62	3.96	4.83	1.09	0.87	0.50	0.08	0.09	0.22	0.33	0.66
SrO	0.96	0.11	0.11	0.45	0.38	0.20	0.39	0.39	0.26	0.11	0.12	0.26	0.20	0.29
BaO	0.19	0.05	0.05	0.16	0.21	0.11	0.05	0.04	0.04	0.01	0.01	0.03	0.03	0.03
Total	100.23	100.42	100.73	100.45	100.42	100.07	100.73	100.85	100.38	100.28	99.80	99.80	99.26	101.10
X_{Or}	7.2	29.5	36.5	30.9	21.7	26.4	6.0	4.7	2.9	0.5	0.5	1.3	1.9	3.7
X_{Ab}	67.8	64.9	59.6	60.5	65.7	65.7	64.3	61.9	47.8	17.0	14.4	48.7	40.9	48.4
X_{An}	20.6	4.9	3.2	5.7	10.0	6.7	28.1	31.9	49.4	83.5	84.8	50.0	57.2	45.9
σX_{An}	0.7	0.9	0.7	0.3	0.4	0.3	0.6	0.5	0.4	1.2	1.3	0.3	0.5	0.8
No. analyses	73	46	25	68	46	57	46	32	88	51	26	22	33	25
							Trace elements in host							
Ba_{calc}*	1440	300	300	960	1250	560	370	420	440	540	540	560	490	460
Ba_{meas}	650	300–550	300–550	460–480	460–480	460–480	370–500	370–500	400	260	260	260	410	410
Sr_{calc}*	1610	140–620	140–620	580–2500	490–2140	250–1120	680	740	570	650	650	730	750	660
Sr_{meas}	930	590	590	950	950	950	550–760	550–760	550	520	520	520	680–690	680–690
References	1	1,3	1,3	1	1	1	2	2	1	1	1	1	1	1

Note: 1 = this study; 2 = Storey et al., 1989; 3 = Katz and Boettcher, 1980. Alkali feldspar: Ba D from Guo et al., 1989, 1992 ($D_{Ba} = 1.5$); Sr D from Henderson, 1982, and Hill, 1978. Plagioclase feldspar: Ba and Sr D from Blundy and Wood, 1991: $RT \ln D_{Sr} = 26800 − 26700X_{An}$, and $RT \ln D_{Ba} = 10200 − 38200X_{An}$. Analytical uncertainty is ±30 ppm for Ba, and ±10 ppm for Sr. Reproducibility for Ba and Sr measurements are 0.55 and 0.57%, respectively (based on ~50 replicates).

TABLE 4. Olivine megacryst analyses

Oxide	Lunar Crater	Dish Hill	San Carlos	Punta Piaxtle	Jumatán	Valle de Santiago 104	Valle de Santiago 152	Valle de Santiago 211
SiO_2	40.6	40.9	40.9	39.5	39.7	39.8	38.2	38.4
Al_2O_3	0.1	0.0	0.0	0.1	0.0	0.0	0.1	0.1
Cr_2O_3	0.08	0.02	0.02	0.00	0.00	—	0.01	—
FeO	10.93	9.97	9.56	16.46	15.35	12.00	21.83	22.33
MnO	0.07	0.16	0.16	0.26	0.25	0.14	0.32	0.31
MgO	47.9	48.4	48.8	43.5	44.1	47.4	38.7	39.0
CaO	0.20	0.07	0.02	0.22	0.25	0.15	0.21	0.21
NiO	0.33	0.34	0.35	0.08	0.04	0.21	0.04	0.04
Total	100.19	99.87	99.88	100.11	99.74	99.82	99.34	100.44
X_{Fo}	89	90	90	82	84	87	76	75
Range	—	88–90	—	81–82	84–85	—	76–81	—

phibolite, amphibole pyroxenite, and feldspar amphibolite (xenoliths: Frey and Prinz, 1978; Wilshire et al., 1980; Nielson and Noller, 1987; Wilshire et al., 1988; McGuire et al., 1991; Wilshire et al., 1991; massifs: Conquere, 1971; Sinigoi et al., 1983). Such veins and pegmatites are commonly preserved only as selvages or at the edge of peridotite xenoliths—that is, they are disaggregated upon eruption. Type II veins (aluminous augite, kaersutite, biotite) are thought to be related to the magmatism that brings them to the surface (Roden et al., 1984; Menzies et al., 1985; Roden and Murthy, 1985).

Type I xenoliths

The Lunar Crater locality has wehrlite (chromian diopside group) and dunite xenoliths (Wilshire et al., 1988). Most other localities (Cima, Dish Hill, San Carlos, San Quintín, and Punta Piaxtle: Wilshire et al., 1988; Frey and Prinz, 1978; Luhr et al., 1992) have lherzolite (chromian diopside group) and websterite xenoliths. The Cima Volcanic Field has an unusual number of composite peridotites, with chromian diopside websterites being the most common host rock for the crosscutting veins and dikes. Recent studies have determined pressures of 7–13 kbar and temperatures of 980–1100 °C for spinel lherzolites from San Carlos, San Quintín, Punta Piaxtle (Kohler and Brey, 1990; Luhr et al., 1992). These P and T conditions are similar to estimates at the Cima localities (900–1100 °C and 8–25 kbar: Wilshire et al., 1991).

MEGACRYSTS

Gabbroic megacrysts

Megacrysts of olivine, augite, and feldspar at the Jumatán and Valle de Santiago are identical in composition to the phases in the gabbroic xenoliths from these localities (see Tables 6 and 7). Megacrysts of olivine, augite,

TABLE 5. Major element analyses of host lavas

Oxide	Lunar Crater	Cima V.F.	Dish Hill	Grand Canyon X-11	San Carlos Flow	San Carlos Scoria	Punta Piaxtle 475	Punta Piaxtle 476	Jumatán 396	Valle de Santiago 103	Valle de Santiago 104	Valle de Santiago 152	Valle de Santiago 14	Valle de Santiago 211
SiO_2	45.6	47.8	45.1	42.9	45.2	45.5	48.2	47.9	47.8	53.9	47.4	46.7	46.3	47.8
TiO_2	2.38	2.01	2.75	3.00	2.38	2.40	2.08	1.94	1.89	1.38	2.58	2.66	3.12	2.81
Al_2O_3	14.9	16.8	14.7	13.4	14.7	14.9	16.7	16.0	17.2	17.7	16.2	16.9	16.6	16.8
Fe_2O_3	3.42	4.80	3.59	4.65	5.09	4.61	2.38	2.87	3.75	3.06	3.76	4.70	4.00	2.43
FeO*	7.99	4.64	7.67	8.37	6.81	7.06	7.44	7.20	6.15	4.88	7.10	7.02	7.45	8.52
MnO	0.21	0.16	0.19	0.18	0.20	0.2	0.18	0.17	0.16	0.12	0.17	0.17	0.17	0.17
MgO	7.8	7.0	7.4	7.9	6.9	6.6	5.5	8.6	7.2	4.3	6.6	6.6	7.1	6.2
CaO	9.91	8.85	9.17	9.54	7.05	7.14	8.08	9.43	10.36	7.24	8.85	8.68	8.98	8.85
Na_2O**	4.26	4.14	4.32	4.97	5.12	4.45	4.6	4.7	3.41	3.86	3.85	3.81	3.35	3.61
K_2O**	2.01	2.03	2.32	2.09	3.27	3.37	2.11	0.55	0.78	1.48	1.59	1.29	1.50	1.48
P_2O_5	0.73	0.54	0.67	0.94	0.91	0.89	0.64	0.46	0.34	0.41	0.60	0.52	0.55	0.50
Total	99.18	98.77	99.12	98.75	97.63	97.12	97.91	99.87	99.04	97.81	98.71	99.22	99.12	99.12
FeO_{tot}	11.07	8.96	10.9	12.55	11.39	11.21	9.58	9.78	9.52	7.63	10.48	11.25	11.05	10.71
ΔNNO (1 bar)	0.51	2.64	0.77	1.25	1.84	1.56	0.14	0.66	1.44	1.11	1.32	1.94	1.41	0.02
ΔNNO (10 kbar)	1.60	3.63	1.81	2.20	2.82	2.59	1.09	1.61	2.59	—	2.27	2.89	1.96	0.97
K_2O/Na_2O	0.47	0.49	0.54	0.42	0.64	0.76	0.46	0.12	0.23	0.38	0.41	0.34	0.45	0.41
Fe^{3+}/Fe^{2+}	0.39	0.93	0.42	0.50	0.67	0.59	0.29	0.36	0.55	0.47	0.48	0.60	0.48	0.26
Mg' (molar)	0.63	0.73	0.67	0.63	0.64	0.63	0.57	0.68	0.68	0.61	0.62	0.63	0.63	0.56
Mt' (wt)	0.49	0.60	0.53	0.49	0.50	0.48	0.43	0.54	0.54	0.47	0.48	0.49	0.49	0.42

* Wet chemical determinations.
** Alkalis determined by flame photometry (except 475 and 476, Punta Piaxtle).

TABLE 6. Gabbro xenolith mineral analyses

Oxide	Valle de Santiago 254B					Valle de Santiago 254D					Jumatán		
	Olivine	Augite	Plag	Mgnt	Ilm	Olivine	Augite	Plag	Mgnt	Ilm	Olivine	Augite	Plag
SiO$_2$	37.5	49.0	53.0	0.08	0.02	37.1	46.6	54.2	0.12	0.03	40.0	51.6	46.6
TiO$_2$	—	1.64	—	15.96	47.29	—	2.36	—	19.24	48.58	—	0.96	—
Al$_2$O$_3$	—	6.2	29.2	6.0	0.6	—	8.4	28.6	7.6	0.7	—	6.0	33.9
Cr$_2$O$_3$	—	0.01	—	0.01	0.00	—	0.00	—	0.00	0.01	—	—	—
V$_2$O$_3$	—	—	—	0.66	0.33	—	—	—	0.58	0.29	—	—	—
Fe$_2$O$_3$	—	3.81	—	32.49	13.49	—	2.19	—	24.95	10.84	—	—	—
FeO	25.88	6.04	0.28	38.68	30.72	30.02	7.58	0.34	42.89	34.11	14.12	5.25	0.37
MnO	0.38	0.19	—	0.38	0.34	0.47	0.21	—	0.44	0.41	0.23	0.07	—
MgO	35.8	13.3	—	5.0	6.4	32.1	11.9	—	4.7	5.1	44.9	15.4	—
CaO	0.07	20.15	12.03	0.02	0.03	0.17	19.44	10.67	0.02	0.03	0.26	20.88	16.74
Na$_2$O	—	0.81	4.32	—	—	—	0.84	5.51	—	—	—	0.47	1.87
K$_2$O	—	—	0.47	—	—	—	—	0.50	—	—	—	—	0.06
SrO	—	—	0.22	—	—	—	—	0.24	—	—	—	—	0.16
BaO	—	—	0.03	—	—	—	—	0.02	—	—	—	—	0.02
Total	99.73	100.80	99.57	99.31	99.29	99.89	100.28	100.21	100.61	100.18	99.60	100.63	99.70
FeO$_{tot}$	—	9.47	—	67.92	42.86	—	9.55	—	65.34	43.87	—	5.25	—
X_{An}	—	—	0.59	—	—	—	—	0.50	—	—	—	—	0.84
Mg' (molar)	0.71	0.80	—	—	—	0.66	0.74	—	—	—	0.84	0.84	—
T (°C)	—	—	—	840		—	—	—	850		—	—	—
ΔNNO	—	—	—	+0.4		—	—	—	0.0		—	—	—

Note: Fe$_2$O$_3$ for Fe-Ti oxides calculated using charge balance and stoichiometry considerations. T and f_{O_2} calculated using Ca-QUIlF equilibria of Frost and Lindsley (1992).

and feldspar occur at the Punta Piaxtle, San Quintín, and Lunar Crater localities (there are no published data on the gabbros from Lunar Crater). Equilibrium crystallization calculations (Ghiorso et al., 1983) indicate that these megacrysts could represent disaggregated gabbroic material that crystallized from the host magma at pressures of 5–15 kbar (Table 8).

Augite. The augite megacrysts from all localities are similar in composition (Table 1). Most are magnesian with values of Mg' [MgO/(MgO + FeO)] varying from 0.75 to 0.90. Augite samples from the Valle de Santiago Maar Field (Appendix 1) have the lowest values of Mg', whereas those from Lunar Crater have the highest. All the augite samples have Al$_2$O$_3$ contents between 6.9 and 10.7 and notable amounts of Na$_2$O (0.85–1.46). The R values [Fe^{3+}/(Fe^{2+} + Fe^{3+})] of augite from a given locality are uniform [Dish Hill = 0.36–0.39; San Carlos

(nos. 1–5) = 0.31–0.38; Mexico = 0.23–0.33], with the exception of Lunar Crater samples, which range from 0.35 to 0.50 (Table 1).

There is much compositional evidence in support of aluminous augite being a high-pressure precipitate. Aluminous augite is a liquidus phase in high-pressure experimental studies of basanites and alkali basalts (Green and Ringwood, 1967; Green and Hibberson, 1970; Thompson, 1974). Sr and Nd isotopic analyses of aluminous augite megacrysts are identical to those of their host lavas at many localities (Stuckless and Irving, 1976; Basu, 1978; Wilkinson and Hensel, 1991). Trace-element partitioning between host lavas and augite is consistent with high-pressure partition coefficients (Irving and Frey, 1984).

The regular solution model SILMIN (Ghiorso et al., 1983) does not predict nonquadrilateral clinopyroxene components (Fe^{3+}, Ti, and Al), which are significant in

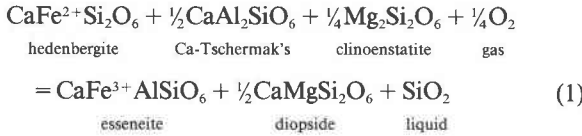**TABLE 7.** Summary table for equilibrium crystallization calculations, gabbro, and megacryst compositions

	Valle de Santiago (152)	Gabbro	Meg.	Jumatán (396)	Gabbro	Meg.	Cima (1633-T)	Gabbro*	Pyrox	Meg.	San Carlos	Gabbro**	Meg.
Wt% H$_2$O	1.0			1.0			1.0				1.0		
P (kbar)	10			10			10				10		
T (°C)	1000			1000			1000				1000		
f_{O_2}	QFM			NNO			QFM				NNO-2		
Fo	67 (79)	64–71	75–76	77 (84)	84	84	69	65–70		—	78 (85)	73	90
An	50	49–59	46–64	54	82–85	50–84	50	48–60	12–60	12	41	61	6–10
100*Mg' (Augite)	80	74–80	80–82	85	84	87	83	—	—	83–85	83		80–82
Oxide	x	x	—	—	—	—	x	x	x	—	x	x	—

Note: values in parentheses indicate liquidus olivine composition. NNO = Ni + nickel oxide buffer; QFM = quartz + fayalite + magnetite buffer. Meg. = megacryst; Pyrox. = pyroxenite.
* Gabbro and pyroxenite data are from Wilshire et al. (1991).
** Gabbro data are from Frey and Prinz (1978).

these augite samples. If the augite megacrysts are cumulates from liquids similar to their host lavas, pyroxene-liquid redox equilibria calculations should be consistent with the redox state of the host lava. As an example of the equilibrium that could exist, we consider the reaction

$$CaFe^{2+}Si_2O_6 + \tfrac{1}{2}CaAl_2SiO_6 + \tfrac{1}{4}Mg_2Si_2O_6 + \tfrac{1}{4}O_2$$

hedenbergite   Ca-Tschermak's   clinoenstatite   gas

$$= CaFe^{3+}AlSiO_6 + \tfrac{1}{2}CaMgSi_2O_6 + SiO_2 \qquad (1)$$

esseneite   diopside   liquid

as a function of temperature and pressure. Entropy, enthalpy, and heat capacity data given by Berman (1988) have been used to calculate the Gibbs free energy of reaction:

$$\Delta G^P_T = \Delta H^0_{298} + \int_{298}^{T} C_P\, dT$$

$$- T\left[\Delta S^0_{298} + \int_{298}^{T} (C_P/T)\, dT\right] + \int_{1}^{P} V\, dP$$

which is then recast as a function of temperature and pressure, as $-\ln K_1 = \Delta G/RT = A/T + B + C(P-1)/T$ where

$$K_1 = \frac{(a_{SiO_2}^{liquid})(a_{CaMgSi_2O_6}^{augite})^{1/2}(a_{CaFeAlSiO_6}^{augite})}{(a_{CaFeSi_2O_6}^{augite})(a_{CaAl_2SiO_6}^{augite})^{1/2}(a_{Mg_2Si_2O_6}^{augite})^{1/4}(f_{O_2})^{1/4}}.$$

The enthalpy and entropy of silica liquid (at 298 K), as well as the entropy, enthalpy, and heat capacity of esseneite, were estimated as described in Appendix 3. Thermodynamic data reported by Bennington et al. (1984) were used for hedenbergite. Esseneite is a naturally occurring pyroxene that contains [6]Fe³⁺ (Cosca and Peacor, 1987). The activities of CaFeSi₂O₆, CaMgSi₂O₆, Mg₂Si₂O₆, CaAl₂SiO₆, and CaFeAlSiO₆ in augite are calculated as follows:

$$a_{CaFeSi_2O_6}^{augite} = \gamma_{CaFeSi_2O_6}^{augite} \cdot X_{Ca}^{M2} \cdot X_{Fe}^{M1} \cdot (X_{Si}^T)^2$$

$$a_{CaMgSi_2O_6}^{augite} = \gamma_{CaMgSi_2O_6}^{augite} \cdot X_{Ca}^{M2} \cdot X_{Mg}^{M1} \cdot (X_{Si}^T)^2$$

$$a_{Mg_2Si_2O_6}^{augite} = \gamma_{Mg_2Si_2O_6}^{augite} \cdot X_{Mg}^{M2} \cdot X_{Mg}^{M1} \cdot (X_{Si}^T)^2$$
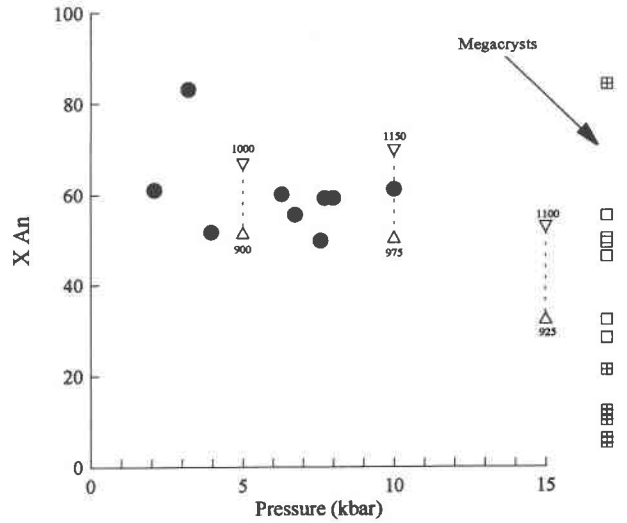
Fig. 3. Gabbro feldspar compositions plotted against pressure (solid circles) as calculated from olivine + augite + magnetite + ilmenite Ca-QUIlF equilibria (Lindsley and Frost, 1992) for gabbro xenoliths from Hawaii (Fodor and Vandermeyden, 1988), San Carlos (Frey and Prinz, 1978), Cima Volcanic Field (Wilshire et al., 1991), and Valle de Santiago Maar Field (this study). Temperatures and f_{O_2} values are constrained by two oxide equilibria, silica activity is constrained by equilibria involving silica, and the uncertainties in the calculated pressures are ±1–3 kbar. Also plotted are feldspar compositional ranges (as a function of temperature in degrees Celsius: triangles) from equilibrium crystallization calculations (SILMIN) on trachybasalt from Valle de Santiago (152), at pressures of 5, 10, and 15 kbar, coexisting with augite and olivine. The megacryst compositional range is shown to the right of the figure (open squares = equilibrium at high pressures; squares with crosses = disequilibrium anorthoclase and bytownite).

$$a_{CaAl_2SiO_6}^{augite} = \gamma_{CaAl_2SiO_6}^{augite} \cdot 4X_{Ca}^{M2} \cdot X_{Al}^{M1} \cdot X_{Al}^T \cdot X_{Si}^T$$

$$a_{CaFe^{3+}AlSiO_6}^{augite} = \gamma_{CaFe^{3+}AlSiO_6}^{augite} \cdot 4X_{Ca}^{M2} \cdot X_{Fe^{3+}}^{M1} \cdot X_{Al}^T \cdot X_{Si}^T \qquad (2)$$

where Fe²⁺ and Mg are distributed in the M1 and M2 sites in accord with bulk Mg/(Mg + Fe²⁺) values. Activity coefficients for diopside, hedenbergite, and enstatite are calculated using relations given by Davidson and Lindsley (1989), whereas those for esseneite and calcium aluminum pyroxene are calculated from the results of

TABLE 8. Summary table for equilibrium crystallization calculations and megacryst compositions

	Lunar Crater	Meg.	Punta Piaxtle	Meg.	San Quintín	Meg.	Dish Hill	Meg.
Wt% H₂O	1.0		1.0		1.0		1.0	
P (kbar)	10		10		10		10	
T (°C)	1000		1025		900		1000	
f_{O_2}	NNO		NNO		QFM		NNO-2	
X_{F_o}	81	90	75 (81)	82	69	—	78 (85)	88–90
X_{An}	48	20–50	49	49	43	28–32	41	—
100*Mg' (Augite)	86	84–90	85	82–85	85	79–82	83	83–86
Oxide	x	—	—	—	x	—	x	—

Note: these localities (except Punta Piaxtle) have gabbro xenoliths, but there are no compositional data for comparison; ( ) indicates liquidus olivine composition; NNO = Ni + nickel oxide buffer; QFM = quartz + fayalite + magnetite buffer; Meg. = megacryst.
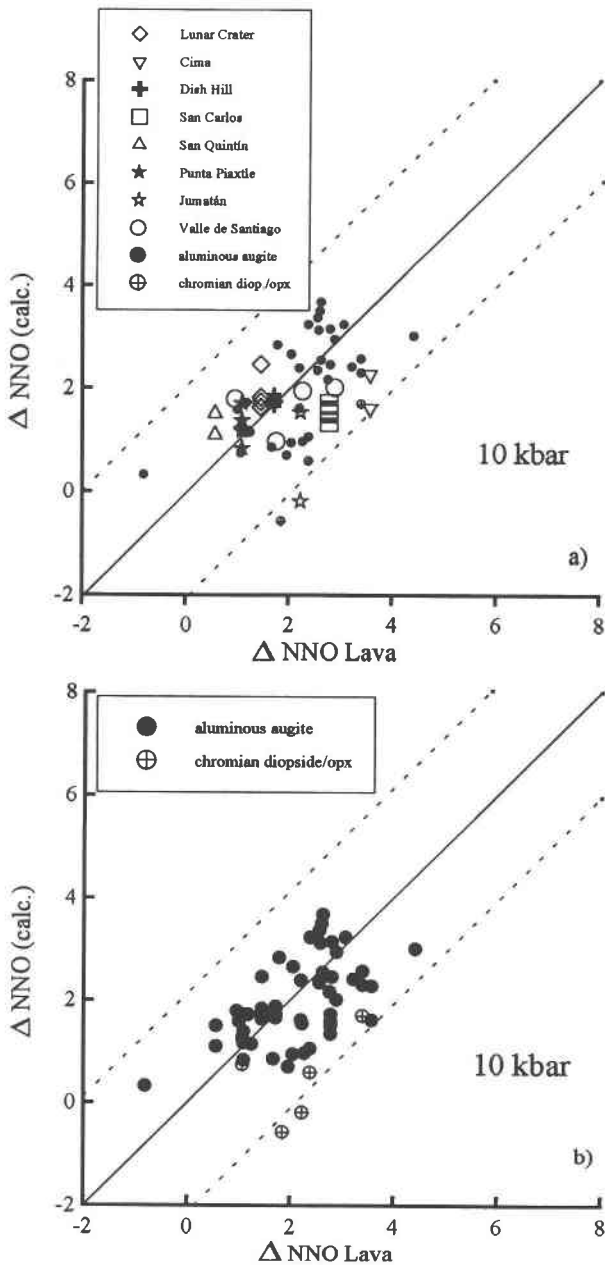
experimental studies as outlined in Appendix 3. The activity of SiO_2 has been calculated using the SILMIN model of Ghiorso et al. (1983). Values for A, B, and C are -12725.50, 4.4786, and 0.1484, respectively ($A = \Delta H/R$, $B = \Delta S/R$, $C = \Delta V/R$). Knowing these parameters together with the activities, one can calculate the f_{O_2} defined by an augite-host pair. Comparison of the f_{O_2} calculated from the augite redox equilibrium (Eq. 1) with the f_{O_2} of the host lava (after Kress and Carmichael, 1991; see Appendix 2) is shown in Figure 4, for calculations at 10 kbar. The error estimates for the augite redox equilibrium calculations are based on uncertainties in the microprobe and XRF analyses (± 0.2 log f_{O_2} units), activity coefficients (± 0.2 log f_{O_2} units), and the free energy data [(± 1.3 log f_{O_2} units) see Fig. 4].

The redox state of the host lavas at most localities leads to f_{O_2} values that are in good agreement with augite redox calculations at 10 kbar. With an increase in pressure, the equiline (1:1) would shift to the right in Figure 4. Figure 4b distinguishes between clinopyroxenes that are aluminous augite and those that are chromian diopside or that occur together with orthopyroxene. That the augite samples that occur with orthopyroxene megacrysts fall on the high pressure side of the equiline (>10 kbar—to the right in Fig. 4), is consistent with the fact that, at higher pressures, orthopyroxene should replace olivine in lavas with this silica activity. This occurs for these lavas at approximately 20 kbar and 1200 °C. The agreement between the two calculated f_{O_2} values indicates that variations in $Fe^{3+}/(Fe^{3+} + Fe^{2+})$ in aluminous augite can be ascribed to pyroxene-melt redox equilibria at high pressures (~ 10 kbar). Notable exceptions are the chromian diopside samples (e.g., Jumatán, Table 1), which have calculated values of $\Delta NNO = 2–3$ units below the equivalence line (Fig. 4). Their redox state is much lower than that of their host lavas.

Feldspar. Recent studies on the partitioning of Sr and Ba between plagioclase and melt (Blundy and Wood, 1991) and alkali feldspar and melt (Guo and Green, 1989, 1992) allow one to examine equilibrium partitioning between the feldspar megacrysts and host lavas of this study. Blundy and Wood (1991) combined experimental and natural data to derive relations for the partitioning of Ba and Sr as a function of T and X_{An} (range of $X_{An} = 0–100$ and $T = 800–1400$ °C) (Table 3). Guo and Green (1989, 1992) reported partition coefficients for Ba between alkali feldspar and melt at 10–25 kbar and 900–1100 °C, for $X_{Or} = 38–61$; they estimated a D_{Ba} (anorthoclase melt) of 1.5, based on these experiments. D_{Sr} (alkali feldspar melt) are taken from studies by Hill (1978) and Henderson (1982). BaO and SrO for feldspar megacrysts and host lavas are reported in Table 3. Using the compositions of the feldspars (X_{An}, wt% SrO, and wt% BaO) and the partitioning expressions presented in these studies (see Table 3), one can calculate how much Sr and Ba (in the host) should be in equilibrium with the feldspar. The Lunar Crater feldspar analyzed in this study is oligoclase; however, an extensive study by Bergman (1982) (see also Schulze, 1987) revealed a population of feldspar megacrysts with

Fig. 4. (a) Comparison of calculated megacryst redox state (Reaction 1) with the host lava redox state. Calculations utilize the augite redox equilibrium (Reaction 1), and the redox state of the host lava (± 0.5 log f_{O_2} units) is calculated at 10 kbar and 1200 °C, using the expression of Kress and Carmichael (1991) (see Appendix 2). The error bars (dashed lines) for the calculated redox state of augite and melt are a combination of factors: analytical data (probe, XRF), free energy data, and activity coefficients. Solid line is 1:1. Augite data from other localities are from Aoki and Kushiro (1968), Best and Brimhall (1974), Binns et al. (1970), Binns (1969), Ghent et al. (1980), Huckenholz (1965a, 1965b), Irving and Frey (1984), Irving (1974), Irving and Green (1976), McGuire (1988), McGuire et al. (1989), and Yoder and Tilley (1962). (b) Same data set as a, except aluminous augite samples are solid symbols, and chromian diopside samples or those augite samples found with orthopyroxene megacrysts are open symbols with crosses.

a larger compositional range, from andesine (An_{50}) to anorthoclase. The SrO and BaO for the andesine (Bergman, 1982), as well as Sr isotopic analyses (Wilshire et al., 1988) of the feldspars and host lavas at Lunar Crater are consistent with equilibrium. San Carlos anorthoclase 3 has low BaO and SrO, consistent with equilibration with the host basanite (Table 3). Feldspar megacrysts from four other localities (Cima, San Quintín, Punta Piaxtle, Valle de Santiago) have BaO and SrO contents consistent with crystallization from an alkali basalt host (see Table 3). BaO and SrO contents of feldspar megacrysts from Jumatán, San Carlos, and Lunar Crater are inconsistent with equilibrium, and they are discussed in the next section.

Hydrous pyroxenite or syenitic megacrysts

The absence of plagioclase feldspar megacrysts at the Dish Hill, Cima V.F., and San Carlos localities rules out the possibility of a gabbroic source for the megacrysts there. The kaersutite and augite megacrysts found there (see also Colville and Novak, 1991) may have come from disaggregated kaersutite ($\pm$ anorthoclase) pyroxenite veins or pegmatites.

Kaersutite. All of the amphiboles analyzed in this study are kaersutite according to the classification of Leake (1978), where molar Ti > 0.50. The kaersutite is fairly homogeneous in major element composition at a given locality, except for variable R [$Fe^{3+}/(Fe^{3+} + Fe^{2+})$] values (Table 2, Fig. 5). Lunar Crater R values range from 0.25 to 0.76, and the San Carlos values from 0.21 to 0.60. The Lunar Crater kaersutite has high Mg', from 0.75 to 0.88, whereas the San Carlos values range from 0.57 to 0.75. Concentrations of F^- and Cl^-, determined by electron microprobe, are low in kaersutite from both localities, ranging from 0.04 and 0.01 at Lunar Crater to 0.08 and 0.01 at San Carlos. This suggests that the OH site is occupied with OH^- or O^{2-} as the dominant species (see also Garcia et al., 1980). Several of the Lunar Crater kaersutite samples contain oriented lamellae of pseudobrookite. One of the San Carlos kaersutite samples (no. 5) contains rounded inclusions of a sulfide mineral that has exsolved into two phases.

R values in kaersutite are inversely correlated with H_2O, suggesting that Fe_2O_3 is produced during dehydration (Boettcher and O'Neil, 1980; Popp and Bryndzia, 1992). Although Dyar et al., (1992) hypothesized that kaersutite R values could be solely due to variations in mantle f_{H_2}, rather than f_{O_2}, there is evidence at Lunar Crater that suggests that high R values in kaersutite (Fig. 5) is a consequence of oxidation as well as dehydration. Pseudobrookite (Fe_2TiO_5) lamellae occur in the kaersutite from Lunar Crater (Table 2); pseudobrookite is stable under oxidizing conditions (near the hematite + magnetite buffer: H + M $\pm$ 1 at 1000 °C), and temperatures >585 °C (Anovitz et al., 1985; Lindsley, 1991). Its presence suggests that oxidation is occurring at >600 °C and near the H + M buffer, several log f_{O_2} units above the redox state of the Lunar Crater basanite (NNO + 0.5).
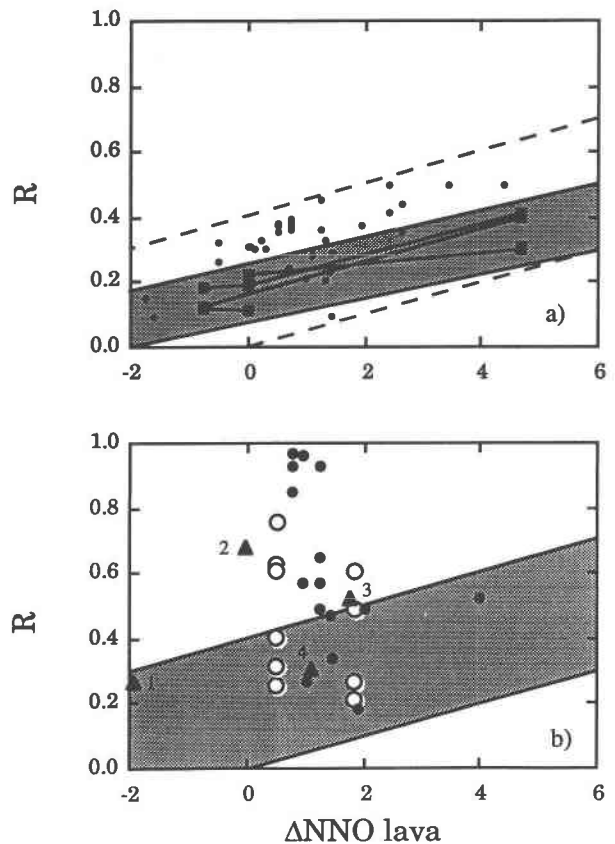
Although a few of the San Carlos and Lunar Crater

Fig. 5. (a) Shaded region represents the range of equilibrium R [$Fe^{3+}/(Fe^{3+} + Fe^{2+})$] values based on those obtained experimentally in calcic amphiboles (Spear, 1981; Clowe et al., 1988; Popp et al., 1992). This equilibrium region is extended to higher values (dashed lines) by including the range of R values for augite megacrysts (and the ΔNNO of their host lava). (b) The R values of kaersutite megacrysts from San Carlos and Lunar Crater (open circles), and Japan, Australia, the Grand Canyon, and Saudi Arabia (solid circles: Wilkinson, 1962; Boettcher and O'Neil, 1980; Aoki, 1963; Irving and Frey, 1984; McGuire et al., 1989; Pallister, 1985; Best and Brimhall, 1974), along with the equilibrium region of a. Triangles are amphibole phenocrysts from flows at (1) Devil's Punchbowl, Mono Craters (Cam-73: Carmichael and Ghiorso, 1990), (2) and (3) Volcán Colima (COL-2 and COL-15: Luhr and Carmichael, 1980; Carmichael, unpublished data), and (4) Valle de Santiago Maar Field, Mexico (GM-103: Tables 2 and 5). Nos. 1, 3, and 4 are amphibole phenocrysts (without reaction rims) in quenched scoria—they plot within the equilibrium region. No. 2 amphibole has opacite reaction rims, and the high R value indicates that oxidation has occurred upon cooling. The ΔNNO is calculated for the host lava using the expression derived by Kress and Carmichael (1991) (see Appendix 2).

kaersutite samples have R values consistent with megacryst-host equilibrium (Fig. 5), isotopic data from these and other localities suggest disequilibrium. The Lunar Crater (Bergman and Foland, 1981; Foland et al., 1983) and San Carlos (Basu, 1978) kaersutite has $^{87}Sr/^{86}Sr$ values that are significantly lower than those of its host lavas
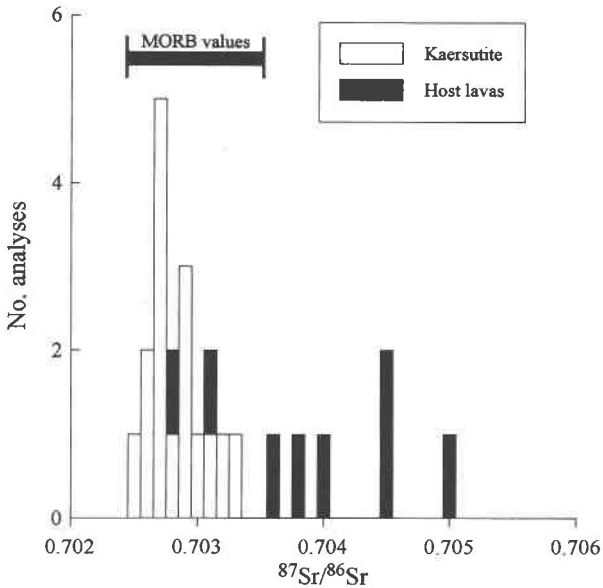
Fig. 6. Histogram of Sr isotope analyses of kaersutite mega-crysts and host lavas from localities in the western U.S., Australia, and Antarctica (data sources are Stuckless and Ericksen, 1976; Basu, 1978; Wilshire et al., 1988; Wilkinson and Hensel, 1991). Range of values for MORB from Basu (1978). The only two host lava values that overlap with the kaersutite values are from Australia (Spring Mount) and Antarctica.

(Fig. 6). In fact, kaersutite megacrysts from all over the world have a narrow range of $^{87}Sr/^{86}Sr$ values, which are similar to the range defined by midocean-ridge basalts (MORB; Fig. 6). The ϵNd measured for three kaersutite megacrysts also fall within the range for MORB, with values of 6.4–7.5 (Wilshire et al., 1988; Wilkinson and Hensel, 1991; Daley and DePaolo, 1992). At most of these localities, the host lavas have higher $^{87}Sr/^{86}Sr$ values (>0.7030), suggesting that the kaersutite crystals are out of equilibrium with the host lavas. Only in a few cases (Spring Mount: Australia and Antarctica) do host lavas have equally low $^{87}Sr/^{86}Sr$ values. Sr isotopic values for kaersutite megacrysts at Dish Hill are identical to those of the vein kaersutite in associated ultramafic xenoliths (Basu, 1978; Wilshire et al., 1980); the megacrysts at Dish Hill and other localities (San Carlos and Lunar Crater) may thus represent disaggregated vein material or kaersutite-bearing Group II pyroxenites or peridotites, both of which occur at these localities (Frey and Prinz, 1978; Wilshire et al., 1988).

Biotite. Biotite megacrysts occur in alkali basalts at several localities throughout the world (see Irving and Frey, 1984). The biotite megacryst from San Carlos contains 7.40 wt% TiO_2, and has a molar Mg' of 0.47 (Table 2). Such TiO_2-rich biotite has been found in hydrous veins in peridotite at San Carlos (Frey and Prinz, 1978). Only three of these megacrysts have been analyzed for Fe^{2+} and Fe_{tot}: those from Murrumburrah (Boettcher and O'Neil, 1980), Rockeskyller (Irving and Frey, 1984), and

San Carlos (Table 2). Some experiments on the R value of biotite as a function of f_{O_2} have been reported by Wones and Eugster (1965). The R value increases with f_{O_2}; all three biotite samples have R values consistent with equilibration at mantle fugacities ($\sim$NNO). Wilkinson and Hensel (1991) measured Sr and Nd isotopic ratios for kaersutite, biotite, anorthoclase megacrysts, and their host analcimite (Spring Mount) and found no significant difference among all the samples, suggesting that these megacrysts may have been derived from veins or pegmatites associated with the alkaline magmatism.

Feldspar. Many feldspar megacrysts have trace-element and Sr and Nd isotopic ratios that are inconsistent with an equilibrium relation with their host lavas. All three of the Jumatán feldspars have too much BaO and SrO to be in equilibrium with the host trachybasalt (Table 3). The high BaO and SrO in anorthoclase and oligoclase (Table 3) megacrysts from Lunar Crater are inconsistent with crystallization from an alkali basalt liquid. San Carlos anorthoclases 1 and 2 (Table 3) contain too much BaO and SrO to be in equilibrium with the host basanite. They may represent disaggregated veins or pegmatites as well. In fact, syenitic xenoliths and plutonic rocks are associated with alkali basalt magmatism in the Galapagos (McBirney and Williams, 1969), Hawaii (Moore et al., 1987), and Tahiti (McBirney and Aoki, 1968). The syenitic material may represent residual liquids from fractionated alkaline magmas. Similar conclusions were drawn in a study of Scottish feldspar megacrysts (Aspen et al., 1990).

Lherzolitic or wehrlitic megacrysts

Several of the Lunar Crater clinopyroxenes and the Jumatán and Punta Piaxtle green clinopyroxenes contain up to 1.1 wt% Cr_2O_3. Our calculations suggest that these minerals could only be in equilibrium with their host lavas at pressures of approximately 30 kbar (Fig. 4), where orthopyroxene is stable; all three of these lavas have olivine and not orthopyroxene megacrysts, suggesting that the diopsides are out of compositional equilibrium with their hosts at 10 kbar. At Lunar Crater, chromian diopside megacrysts are identical in composition to chromian diopside in the Type I peridotite xenoliths (Bergman, 1982). For these reasons, it can be concluded that chromian diopside megacrysts are derived from disaggregated Type I peridotite xenoliths.

Olivine megacrysts from San Carlos and Dish Hill are too magnesian to be in equilibrium with their host lavas (see results of calculations in Tables 7 and 8). Although the Dish Hill olivine is close to the calculated equilibrium olivine, its major- and minor-element contents (NiO = 0.34; CaO = 0.07) are identical to those reported for olivine from a lherzolite at this locality (sample 32-22: Wilshire et al., 1988). The Dish Hill olivines may then be xenocrysts derived from dunite and wehrlite xenoliths that are present in the same host lava (Wilshire and Shervais, 1975; Wilshire et al., 1988). The San Carlos olivines may similarly be derived from disaggregated Type I pe-

ridotite or dunite xenoliths at this locality (Wilshire et al., 1988).

SUMMARY

All of the megacrysts in this study represent xenocrysts; none of them has crystallized directly from the host basalt. The augite, olivine, and feldspar megacryst assemblages at Lunar Crater, Cima V.F., San Carlos, San Quintín, Punta Piaxtle, Jumatán, and Valle de Santiago can be attributed to disaggregated gabbroic and pyroxenitic material, from pressures of 5–15 kbar. Augite, kaersutite, biotite, and anorthoclase megacrysts from San Carlos, Lunar Crater, and Dish Hill may have formed in disrupted Type II mantle veins or pegmatites. Magnesian olivine (Fo_{89-90}) and chromian diopside megacrysts at Lunar Crater, San Carlos, Punta Piaxtle, and Jumatán must be derived from Type I, chromian diopside lherzolite and wehrlite.

REFERENCES CITED

Anovitz, L.M., Treiman, A.H., Essene, E.J., Hemingway, B.S., Westrum, E.F., Wall, V.J., Burriel, R., and Bohlen, S.R. (1985) The heat capacity of ilmenite and phase equilibria in the system Fe-Ti-O. Geochimica et Cosmochimica Acta, 49, 2027–2040.

Aoki, K. (1963) The kaersutites and oxykaersutites from alkalic rocks of Japan and surrounding areas. Journal of Petrology, 4, 198–210.

———(1970) Andesine megacrysts in alkali basalts from Japan. Contributions to Mineralogy and Petrology, 25, 284–288.

Aoki, K., and Kushiro, I. (1968) Some clinopyroxenes from ultramafic inclusions in Dreiser Weiher, Eifel. Contributions to Mineralogy and Petrology, 18, 326–337.

Aspen, P., Upton, B.G.J., and Dickin, A.P. (1990) Anorthoclase, sanidine and associated megacrysts in Scottish Alkali basalts: High-pressure syenitic debris from upper mantle sources? European Journal of Mineralogy, 2, 503–517.

Bacon, C.R., and Carmichael, I.S.E. (1973) Stages in the P-T path of ascending basalt magma: An example from San Quintín, Baja California. Contributions to Mineralogy and Petrology, 41, 1–22.

Basu, A.R. (1978) Trace elements and Sr-isotopes in some mantle-derived hydrous minerals and their significance. Geochimica et Cosmochimica Acta, 42, 659–668.

Bennington, K.O., Bayer, R.P., and Brown, R.R. (1984) Thermodynamic properties of hedenbergite, a complex silicate of Ca, Fe, Mn and Mg. U.S. Bureau of Mines Report of Investigations, 8873, 19 p.

Bergman, S.C. (1982) Petrogenetic aspects of the alkali-basaltic lavas and included megacrysts and nodules from the Lunar Crater Volcanic Field, Nevada, USA. Ph.D. thesis, Princeton University, Princeton, New Jersey.

Bergman, S.C., and Foland, K.A. (1981) Origin of Cr-rich and Ti-rich clinopyroxene megacrysts from basanites of the Lunar Crater Volcanic Field, Nevada (abs.). Eos, 62, 415.

Berman, R.G. (1988) Internally-consistent thermodynamic data for minerals in the system $Na_2O-K_2O-CaO-MgO-FeO-Fe_2O_3-Al_2O_3-SiO_2TiO_2-H_2O-CO_2$. Journal of Petrology, 29, 445–522.

Best, M.G., and Brimhall, W.H. (1974) Late Cenozoic alkali basaltic magmas in the western Colorado Plateaus and the Basin and Range Transition Zone, USA, and their bearing on mantle dynamics. Geological Society of America Bulletin, 85, 1677–1690.

Binns, R.A. (1969) High-pressure megacrysts in basanitic lavas near Armidale, New South Wales. American Journal of Science, 267A, 33–49.

Binns, R.A., Duggan, M.B., Wilkinson, J.F.G., and Kalocsai, G.I.Z. (1970) High pressure megacrysts in alkaline lavas from northeastern New South Wales. American Journal of Science, 269, 132–168.

Blundy, J.D., and Wood, B.J. (1991) Crystal-chemical controls on the partitioning of Sr and Ba between plagioclase feldspar, silicate melts, and hydrothermal solutions. Geochimica et Cosmochimica Acta, 55, 193–210.

Boettcher, A.L., and O'Neil, J.R. (1980) Stable isotope, chemical and petrographic studies of high-pressure amphiboles and micas: Evidence for metasomatism in the mantle source regions of alkali basalts and kimberlites. American Journal of Science, 280A, 594–621.

Buenig, D.K., and Buseck, P.R. (1973) Fe-Mg lattice diffusion in olivine. Journal of Geophysical Research, 78, 6852–6862.

Carmichael, I.S.E., and Ghiorso, M.S. (1990) The effect of oxygen fugacity on the redox state of natural liquids and their crystallizing phases. In Mineralogical Society of America Reviews in Mineralogy, 24, 191–212.

Carmichael, I.S.E., Nicholls, J., Spera, F.J., Wood, B.J., and Nelson, S.A. (1977) High-temperature properties of silicate liquids: Applications to the equilibrium and ascent of basic magma. Philosophical Transactions of the Royal Society of London, 286A, 373–431.

Cashman, K.V., and Marsh, B.D. (1988) Crystal size distribution (CSD) in rocks and the kinetics and dynamics of crystallization. II. Makaopuhi lava lake. Contributions to Mineralogy and Petrology, 99, 292–305.

Christie, D.M., Carmichael, I.S.E., and Langmuir, C.H. (1986) Oxidation states of mid-ocean ridge basalt glasses. Earth and Planetary Science Letters, 79, 397–411.

Clowe, C.A., Popp, R.K., and Fritz, S.J. (1988) Experimental investigation of the effect of oxygen fugacity on ferric-ferrous ratios and unit-cell parameters of four natural clinoamphiboles. American Mineralogist, 73, 487–499.

Colville, A.A., and Novak, G.A. (1991) Kaersutite megacrysts and associated crystal inclusions from the Cima Volcanic Field, San Bernardino County, California. Lithos, 27, 107–114.

Conquere, F. (1971) Amphibole pyroxenites from Lherz. Contributions to Mineralogy and Petrology, 33, 32–61.

Cosca, M.A., and Peacor, D.R. (1987) Chemistry and structure of esseneite ($CaFe^{3+}AlSiO_6$), a new pyroxene produced by pyrometamorphism. American Mineralogist, 72, 148–156.

Daley, E.E., and DePaolo, D.J. (1992) Isotopic evidence for lithospheric thinning during extension: Southeastern Great Basin. Geology, 20, 104–108.

Davidson, P.M., and Lindsley, D.L. (1989) Thermodynamic analysis of pyroxene-olivine-quartz equilibria in the system $CaO-MgO-FeO-SiO_2$. American Mineralogist, 74, 18–30.

Dyar, M.D., McGuire, A.V., and Mackwell, S.J. (1992) Fe^{3+}/H^+ and D/H in kaersutites: Misleading indicators of mantle source fugacities. Geology, 20, 565–568.

Fodor, R.V., and Vandermeyden, H.J. (1988) Petrology of gabbroic xenoliths from Mauna Kea Volcano, Hawaii. Journal of Geophysical Research, 93, 4435–4452.

Foland, K.A., Bergman, S.C., Hofmann, A.W., and Raczek, I. (1983) Nd and Sr isotopic variations in alkali basalts and megacrysts from the Lunar Crater Volcanic Field, Nevada (abs.). Eos, 64, 338.

Frey, F.A., and Prinz, M. (1978) Ultramafic inclusions from San Carlos, Arizona: Petrologic and geochemical data bearing on their petrogenesis. Earth and Planetary Science Letters, 38, 129–176.

Frost, B.R., and Lindsley, D.L. (1992) Equilibria among Fe-Ti oxides, pyroxenes, olivine, and quartz. II. Applications. American Mineralogist, 77, 1004–1020.

Garcia, M.O., Muenow, D.W., and Liu, N.W.K. (1980) Volatiles in Ti-rich amphibole megacrysts, southwest USA. American Mineralogist, 65, 306–312.

Gastil, G., Krummenacher, D., and Jensky, W.A. (1978) Reconnaissance geology of west-central Nayarit, Mexico. Geological Society of America Map MC-24, scale 1:200 000.

Ghent, E.D., Coleman, R.G., and Hadley, D.G. (1980) Ultramafic inclusions and host alkali-olivine basalts of the southern coastal plain of the Red Sea, Saudi Arabia. American Journal of Science, 280-A, 499–527.

Ghiorso, M.S., Carmichael, I.S.E., Rivers, M.L., and Sack, R.O. (1983) The Gibbs free energy of mixing of natural silicate liquids: An expanded regular solution approximation for the calculation of magmatic intensive variables. Contributions to Mineralogy and Petrology, 84, 107–145.

Green, D.H., and Hibberson, W. (1970) Experimental duplication of conditions of precipitation of high-pressure phenocrysts in a basaltic magma. Physics of the Earth and Planetary Interiors, 3, 247–254.

Green, D.H., and Ringwood, A.E. (1967) The genesis of basaltic magmas. Contributions to Mineralogy and Petrology, 15, 103–190.

Grove, T.L. (1978) Cooling histories of Luna 24 very low Ti ferrobasalts: An experimental study. Proceedings of the 9th Lunar and Planetary Science Conference, 565–584.

Grove, T.L., and Juster, T.C. (1989) Experimental investigations of low-Ca pyroxene stability and olivine-pyroxene-liquid equilibria at 1 atm in natural basaltic and andesitic liquids. Contributions to Mineralogy and Petrology, 103, 287–305.

Grove, T.L., Kinzler, R.J., and Bryan, W.B. (1990) Natural and experimental phase relations of lavas from Serocki Volcano. Proceedings of the Ocean Drilling Project, Scientific Results, 106/109, 9–17.

Guo, J.F., and Green, T.H. (1989) Ba partitioning between alkali-feldspar and silicate melts at high temperature and pressure. Contributions to Mineralogy and Petrology, 102, 328–335.

Guo, J.F., Green, T.H., and O'Reilly, S.Y. (1992) Ba partitioning and the origin of anorthoclase megacrysts in basaltic rocks. Mineralogical Magazine, 56, 101–107.

Hasenaka, T., and Carmichael, I.S.E. (1987) The cinder cones of Michoacan-Guanajuato, central Mexico: Petrology and chemistry. Journal of Petrology, 28, 241–269.

Henderson, P. (1982) Inorganic geochemistry, 353 p. Pergamon, New York.

Hill, P.E. (1978) Experimental determinations of partition coefficients for Rb, Sr and Ba between alkali feldspar and silicate liquid. Geochimica et Cosmochimica Acta, 42, 833–846.

Huckenholz, H.G. (1965a) Der petrogenetische Werdegang der Klinopyroxene in den tertiaren Vulkaniten der Hocheifel I. Beitrage zur Mineralogie und Petrographie, 11, 138–195.
———(1965b) Der petrogenetische Werdegang der Klinopyroxene in den tertiaren Vulkaniten der Hocheifel II. Beitrage zur Mineralogie und Petrographie, 11, 415–448.

Irving, A.J. (1974) Megacrysts from the Newer Basalts and other basaltic rocks of southeastern Australia. Geological Society of America Bulletin, 85, 1503–1514.

Irving, A.J., and Frey, F.A. (1984) Trace element abundances in megacrysts and their host basalts: Constraints on partition coefficients and megacryst genesis. Geochimica et Cosmochimica Acta, 48, 1201–1221.

Irving, A.J., and Green, D.H. (1976) Geochemistry and petrogenesis of newer basalts of Victoria and southeast Australia. Journal of the Geological Society of Australia, 23, 45–66.

Juster, T.C., Grove, T.L., and Perfit, M.R. (1990) Experimental constraints on the generation of FeTi basalts, andesites and rhyodacites at the Galapagos Spreading Center, 85°W and 95°W. Journal of Geophysical Research B, 94, 9251–9274.

Katz, M., and Boettcher, A. (1980) The Cima Volcanic Field. In D.L. Fife and A.R. Brown, Eds., Geology and mineral wealth of the California desert, p. 236–241. South Coast Geological Society, Santa Ana, California.

Kennedy, A.K., Grove, T.L., and Johnson, R.W. (1990) Experimental and major element constraints on the evolution of lavas from Lihir Island, Papua New Guinea. Contributions to Mineralogy and Petrology, 104, 722–734.

Kirkpatrick, R.J. (1975) Crystal growth from the melt: A review. American Mineralogist, 60, 798–814.

Kirkpatrick, R.J., Robinson, G.R., and Hays, J.F. (1976) Kinetics of crystal growth from silicate melts: Anorthite and diopside. Journal of Geophysical Research, 81, 5715–5720.

Kohler, T.P., and Brey, G.P. (1990) Calcium exchange between olivine and clinopyroxene calibrated as a geothermobarometer for natural peridotites from 2 to 60 kb with applications. Geochimica et Cosmochimica Acta, 54, 2375–2388.

Kress, V.C., and Carmichael, I.S.E. (1991) The compressibility of silicate liquids containing Fe_2O_3 and the effect of composition, temperature, oxygen fugacity and pressure on their redox states. Contributions to Mineralogy and Petrology, 108, 82–92.

Leake, B.L. (1978) Nomenclature of amphiboles. American Mineralogist, 63, 1023–1052.

LeMaitre, R.W. (1965) The significance of the gabbroic xenoliths from Gough Island, South Atlantic. Mineralogical Magazine, 34, 303–317.

Lindsley, D.L. (1991) Experimental studies of oxide minerals. In Mineralogical Society of America Reviews in Mineralogy, 25, 69–106.

Lindsley, D.L., and Frost, B.R. (1992) Equilibria among Fe-Ti oxides, pyroxenes, olivine, and quartz. I. Theory. American Mineralogist, 77, 987–1003.

Lofgren, G.E. (1990) Rapid growth of megacrysts: Dynamic crystallization of melts of nearly monomineralic composition. Geological Society of America Abstracts with Programs, 22, A164.

Luhr, J.F., and Carmichael, I.S.E. (1980) The Colima Volcanic Complex, Mexico. I. Post-caldera andesites from Volcán Colima. Contributions to Mineralogy and Petrology, 71, 343–372.

Luhr, J.F., Aranda-Gomez, J.J., and Pier, J.G. (1992) T-P-f_{O_2}-texture relationships among peridotite xenoliths from the Mexican Basin and Range Province (abs.). Eos, 73, 650.

Marsh, B.D., Gunnarsson, B., Congdon, R., and Carmody, R. (1991) Hawaiian basalt and Icelandic rhyolite: Indicators of differentiation and partial melting. Geologische Rundschau, 80, 481–510.

Mahood, G.A., and Baker, D.R. (1986) Experimental constraints on depths of fractionation of mildly alkalic basalts and associated felsic rocks: Pantelleria, Strait of Sicily. Contributions to Mineralogy and Petrology, 93, 251–264.

McBirney, A.R., and Aoki, K. (1968) Petrology of the Island of Tahiti. Geological Society of America Memoir, 116, 523–556.

McBirney, A.R., and Williams, H. (1969) Geology and Petrology of the Galapagos Islands. Geological Society of America Memoir, 118, 197 p.

McGuire, A.V. (1988) The mantle beneath the Red Sea margin: Xenoliths from western Saudi Arabia. Tectonophysics, 150, 101–120.

McGuire, A.V., Dyar, M.D., and Ward, K.A. (1989) Neglected Fe^{3+}/Fe^{2+} ratios: A study of Fe^{3+} content of megacrysts from alkali basalts. Geology, 17, 687–690.

McGuire, A.V., Dyar, M.D., and Nielson, J.E. (1991) Metasomatic oxidation of upper mantle peridotite. Contributions to Mineralogy and Petrology, 109, 252–264.

Menzies, M.A., Kempton, P.D., and Dungan, M. (1985) Interaction of continental lithosphere and asthenosphere melts below the Geronimo Volcanic Field. Journal of Petrology, 26, 663–693.

Moore, R.B., Clague, D.A., Rubin, M., and Bohrson, W.A. (1987) Hualalai Volcano: A preliminary summary of geologic, petrologic and geophysical data. U.S. Geological Survey Professional Paper, 1350, 571–585.

Morse, S.A. (1980) Kiglapait Mineralogy. II. Fe-Ti oxide minerals and the activities of oxygen and silica. Journal of Petrology, 21, 685–719.

Murphy, G.P. (1986) The chronology, pyroclastic stratigraphy and petrology of the Valle de Santiago Maar Field, Central Mexico, 55 p. M.S. thesis, University of California, Berkeley.

Nielson, J.E., and Noller, J.S. (1987) Processes of mantle metasomatism: Constraints from observations of composite peridotite xenoliths. In Geological Society of America Special Paper, 215, 61–76.

Pallister, J.S. (1985) Reconnaissance geology of the Harrat Hutaymah Quadrangle, Sheet 26/42A Kingdom of Saudi Arabia. U.S. Geological Survey Open File Report, 85-125, 77 p.

Popp, R.K., and Bryndzia, L.T. (1992) Statistical analysis of Fe^{3+}, Ti, and OH in kaersutite from alkalic igneous rocks and mafic mantle xenoliths. American Mineralogist, 77, 1250–1257.

Popp, R.K., Virgo, D., Hoering, T.C., and Phillips, M.W. (1992) Experimental investigation of ferric-ferrous ratios in kaersutitic amphiboles (abs.). Eos, 73, 337.

Richet, P., Bottinga, Y., Denielou, L., Petitet, J.P., and Tequi, C. (1982) Thermodynamic properties of quartz, cristobalite and amorphous SiO_2: Drop calorimetry measurements between 1000 and 1800 K and a review from 0 to 2000 K. Geochimica et Cosmochimica Acta, 46, 2639–2658.

Roden, M.F., and Murthy, V.R. (1985) Mantle metasomatism. Annual Reviews of Earth and Planetary Science, 13, 269–296.

Roden, M.F., Frey, F.A., and Francis, D.M. (1984) An example of consequent mantle metasomatism in peridotite inclusions from Nunival Island, Alaska. Journal of Petrology, 25, 546–577.

Rutherford, M.J., and Hermes, O.D. (1984) Melatroctolite-anorthositic gabbro complex, Cumberland, Rhode Island: Petrology, origin and regional setting. Geological Society of America Bulletin, 95, 844–854.

Sack, R.O., Walker, D., and Carmichael, I.S.E. (1987) Experimental petrology of alkalic lavas: Constraints on cotectics of multiple saturation in natural basic liquids. Contributions to Mineralogy and Petrology, 96, 1–23.

Schulze, D.J. (1987) Megacrysts from alkalic volcanic rocks. In P.H. Nixon, Ed., Mantle xenoliths, 844 p. Wiley, New York.

Sinigoi, S., Comin-Chiaramonti, P., Demarchi, G., and Siena, F. (1983) Differentiation of partial melts in the mantle: Evidence from the Balmuccia peridotite, Italy. Contributions to Mineralogy and Petrology, 82, 351–359.

Spear, F.S. (1981) An experimental study of hornblende stability and compositional variability in amphiboles. American Journal of Science, 281, 697–734.

Spera, F.J. (1984) Carbon dioxide in petrogenesis. III. Role of volatiles in the ascent of alkaline magma with special reference to xenolith-bearing mafic lavas. Contributions to Mineralogy and Petrology, 88, 217–232.

Stebbins, J.F., Carmichael, I.S.E., and Moret, L.K. (1984) Heat capacities and entropies of silicate liquids and glasses. Contributions to Mineralogy and Petrology, 86, 131–148.

Storey, M., Rogers, G., Saunders, A.D., and Terrel, D.J. (1989) San Quintín volcanic field, Baja California, Mexico: 'Within plate' magmatism following ridge subduction. Terra Research, 22, 195–202.

Stuckless, J.S., and Ericksen, R.L. (1976) Strontium isotope geochemistry of the volcanic rocks and associated megacrysts and inclusions from Ross Island and vicinity, Antarctica. Contributions to Mineralogy and Petrology, 58, 111–126.

Stuckless, J.S., and Irving, A.J. (1976) Strontium isotope geochemistry of megacrysts and host basalts from southeastern Australia. Geochimica et Cosmochimica Acta, 40, 209–213.

Thompson, R.N. (1974) Some high-pressure pyroxenes. Mineralogical Magazine, 39, 768–787.

Tormey, D.R., Grove, T.L., and Bryan, W.B. (1987) Experimental petrology of normal MORB near the Kane Fracture Zone: 22°–25°N, Mid-Atlantic Ridge. Contributions to Mineralogy and Petrology, 96, 121–139.

Tsuchiyama, A. (1986) Experimental study of olivine-melt reaction and its petrological implications. Journal of Volcanology and Geothermal Research, 29, 245–264.

Upton, B.G.J., and Wadsworth, W.J. (1972) Peridotitic and gabbroic rocks associated with the shield-forming lavas of Reunion. Contributions to Mineralogy and Petrology, 35, 139–158.

Walker, D., Kirkpatrick, R.J., Longhi, J., and Hays, J.F. (1976) Crystallization history of lunar picritic basalt sample 12002: Phase equilibria and cooling rate studies. Geological Society of America Bulletin, 87, 646–656.

Wiebe, R.A., and Snyder, D. (1993) Slow, dense replenishment of a basic magma chamber: The Layered Series of the Newark Island layered intrusion, Nain, Labrador. Contributions to Mineralogy and Petrology, 113, 59–72.

Wilkinson, J.F.G. (1962) Mineralogical, geochemical and petrogenetic aspects of an analcite-basalt from the New England district of New South Wales. Journal of Petrology, 3, 192–214.

Wilkinson, J.F.G., and Hensel, H.D. (1991) An analcime mugearite-megacryst association from north-eastern New South Wales: Implications for high-pressure amphibole-dominated fractionation of alkaline magmas. Contributions to Mineralogy and Petrology, 109, 240–251.

Wilkinson, J.F.G., and LeMaitre, R.W. (1987) Upper mantle amphiboles and micas and TiO_2, K_2O and P_2O_5 abundances and $100*Mg/(Mg + Fe^{2+})$ ratios of common basalts and andesites: Implications for modal mantle metasomatism and undepleted mantle compositions. Journal of Petrology, 28, 37–73.

Wilshire, H.G., and Binns, R.A. (1961) Basic and ultrabasic xenoliths from volcanic rocks of New South Wales. Journal of Petrology, 2, 185–208.

Wilshire, H.G., and Shervais, J.W. (1975) Al-augite and Cr-diopside ultramafic xenoliths in basaltic rocks from western United States. Physics and Chemistry of the Earth, 9, 257–272.

Wilshire, H.G., Nielson Pike, J.E., Meyer, C.E., and Schwarzman, E.C. (1980) Amphibole-rich veins in lherzolite xenoliths, Dish Hill and Deadman Lake, California. American Journal of Science, 280A, 576–593.

Wilshire, H.G., Meyer, C.E., Nakata, J.K., Calk, L.C., Shervais, J.W., Nielson Pike, J.E., and Schwarzman, E.C. (1988) Mafic and ultramafic xenoliths from volcanic rocks of the western United States. U.S. Geological Survey Professional Paper, 1143, 179 p.

Wilshire, H.G., McGuire, A.V., Noller, J.S., and Turrin, B.D. (1991) Petrology of lower crustal and upper mantle xenoliths from the Cima Volcanic Field, California. Journal of Petrology, 32, 169–200.

Wilson, A.D. (1955) Determination of ferrous iron in rocks and minerals. Bulletin of the Geological Survey of Great Britain, 9, 56–58.

Wones, D.R., and Eugster, H.P. (1965) Stability of biotite: Experiment, theory and application. American Mineralogist, 50, 1228–1272.

Yoder, H.S., Jr., and Tilley, C.E. (1962) Origin of basaltic magmas: An experimental study of natural and synthetic rock systems. Journal of Petrology, 3, 342–532.

APPENDIX 1: SAMPLE LOCALITIES

Easy Chair Crater, Lunar Crater Volcanic Field, Nevada
Basanite host; augite, kaersutite, plagioclase, olivine megacrysts; mafic and ultramafic xenoliths; Wilshire et al. (1988).

Cima Volcanic Field, southeast California (cone 1633 T)
Trachybasalt host; augite, kaersutite, and feldspar megacrysts; mafic and ultramafic xenoliths; Wilshire et al. (1988).

Dish Hill, southeast California
Basanite host; augite, kaersutite, olivine, and spinel megacrysts; mafic and ultramafic xenoliths; Wilshire et al. (1988).

Peridot Mesa, San Carlos, Arizona
Basanite host; augite, kaersutite, anorthoclase, olivine, and phlogopite megacrysts; mafic and ultramafic xenoliths; Wilshire et al. (1988).

San Quintín, Baja California, Mexico
Alkali basalt host; plagioclase and augite megacrysts; mafic and ultramafic xenoliths; Bacon and Carmichael (1973), Basu (1978).

Punta Piaxtle, Sinaloa, Mexico
Alkali basalt host; augite, feldspar, and olivine megacrysts; mantle xenoliths.

Jumatán Falls, Nayarit, Mexico (396)
Trachybasalt host; augite, olivine, and feldspar megacrysts; mafic xenoliths; Gastil et al. (1978).

Valle de Santiago Maar Field, central Mexico
Alkali basalt host [Maars Hoya Alverez (14, 229), San Nicholas (103, 104), Cintura (152), and Rancho Unidos flow (211)]; plagioclase, augite, and olivine

megacrysts; gabbroic and troctolitic xenoliths; Murphy (1986), Hasenaka and Carmichael (1987)

APPENDIX 2: MINERAL AND HOST LAVA ANALYSES

Individual augite and kaersutite megacrysts were crushed and sieved to a 45–80 mesh size and then magnetically separated and hand-picked under a stereoscope. Mineral separates were ultrasonically cleaned in distilled H_2O and washed in acetone. These grains were then analyzed by electron microprobe. The ARL-SEMQ microprobe at the University of California, Berkeley, has eight channels, with a 52.5° take-off angle. Operating conditions were 15-kV accelerating voltage, 30-nA sample current, and 10-s counting times. Ten to 30 10-s analyses from a given area are averaged together. Standards used include a variety of synthetic (TiO_2, Mg_2SiO_4, and Fe_2SiO_4) and natural (kaersutite, diopside, rhodonite, and jadeite) materials. The mineral analyses presented in Tables 1–4 are averages of three point scans (10–30 points per scan). Traverses were conducted on individual grains to detect compositional zoning. Kaersutite, feldspar, and augite megacrysts that were analyzed in greater detail are compositionally homogeneous (Fig. 2). Host lavas were powdered in a tungsten carbide shatterbox for 1 min and then fused with lithium tetraborate flux into glass disks for analysis by X-ray fluorescence (XRF) spectroscopy. Standards used in XRF spectroscopy include six samples that were analyzed using wet-chemical techniques ranging from alkali basalt to rhyolite. Both the mineral separates and lava powders were analyzed for Fe^{2+} using a modified version of the technique described by Wilson (1955). Rock powders were analyzed for Na_2O and K_2O by flame photometry.

Host lavas

Major-element analyses of all host lavas are presented in Table 5. The lavas from Dish Hill, San Carlos, and Lunar Crater are all basanites with 7.4–8.6 wt% total alkalis at SiO_2 of ~45.5 wt%. The Fe^{3+}/Fe^{2+} values range from 0.39 to 0.67, and Mg' values are less variable from 0.63 to 0.67 (Table 5). The lavas from Cima V.F. and Mexico (San Quintín, Jumatán, and Valle de Santiago) contain lower alkalis, from 5.1 to 6.2 at 46–47 wt% SiO_2, and are trachybasalts. Their Mg' values overlap those of the western U.S. samples, from 0.62 to 0.63.

ΔNNO

The f_{O_2} of natural lavas has been calibrated as a function of temperature, pressure, composition, and Fe^{3+}/Fe^{2+} ratio (Kress and Carmichael, 1991):

$$\ln\left(\frac{X_{Fe_2O_3}}{X_{FeO}}\right) = a\ln(f_{O_2}) + b/T + c + \sum_i d_i X_i$$
$$+ e\left[1 - \frac{T_0}{T} - \ln\left(\frac{T}{T_0}\right)\right] + f\frac{P}{T}$$
$$+ g\frac{(T - T_0)P}{T} + h\frac{P^2}{T}.$$

The redox state of a natural lava (above the liquidus) does not change relative to an O buffer such as NNO (Ni + nickel oxide) with changes in temperature, thus allowing one to calculate the redox state of a lava relative to such a buffer at a nominal temperature (Kress and Carmichael, 1991); this relative value is referred to as ΔNNO (calculated here at 1200 °C). If the magma was closed to O during ascent and eruption, then the ΔNNO value represents the redox state of the liquid before eruption. The San Carlos lava flow and scoria samples have the same value of ΔNNO, indicating that no oxidation has occurred during the pyroclastic eruption, as opposed to the flow. The redox state of these lavas (calculated at 1 bar) ranges from ΔNNO = 0–2.6 (Table 5), which is significantly more oxidized than midocean-ridge basalts (ΔNNO = −3–0; Christie et al., 1986).
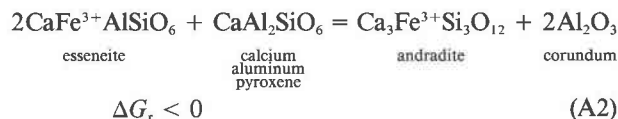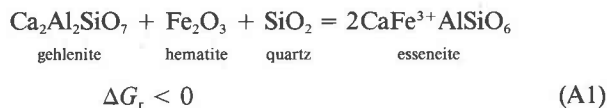
APPENDIX 3: THERMODYNAMIC ESTIMATES

1. Thermodynamic data for esseneite were estimated as follows (using data from Berman, 1988):

Entropy and heat capacity

S^0_{298} (esseneite) = S^0_{298} (calcium aluminum pyroxene)

$+ \frac{1}{2}S^0_{298}$ (hematite)

$- \frac{1}{2}S^0_{298}$ (corundum)

$= 159.06$ J/(mol·K).

Enthalpy

The following two bracketing reactions are utilized to calculate the enthalpy of esseneite. The Gibbs free energy of both reactions must be negative:

$Ca_2Al_2SiO_7 + Fe_2O_3 + SiO_2 = 2CaFe^{3+}AlSiO_6$
gehlenite   hematite   quartz   esseneite

$\Delta G_r < 0$ (A1)

$2CaFe^{3+}AlSiO_6 + CaAl_2SiO_6 = Ca_3Fe^{3+}Si_3O_{12} + 2Al_2O_3$
esseneite   calcium aluminum pyroxene   andradite   corundum

$\Delta G_r < 0$ (A2)

The free energy of esseneite must be < −2693.02 kJ/mol (A1), and > −2712.07 kJ/mol (A2) in order for esseneite to be stable. These two reactions must be spontaneous, as we don't find melilite-bearing granites (A1), and esseneite and calcium aluminum pyroxene are not stable, separate phases at 298 K and 1 bar (A2). The average of these two bracketing values, $\Delta G_{298} = -2702.54$ kJ/mol, in combination with S_{298} (esseneite) = 159.06 J/(mol·K), is then used to calculate the enthalpy of esseneite, $\Delta H_{298} = -2873.14$ kJ/mol.

2. The enthalpy and entropy of silica liquid (at 298 K) were estimated relative to cristobalite (Berman, 1988), using the heat of fusion of cristobalite (Richet et al., 1982) and the heat capacity of silica glass (Stebbins et al., 1984) as follows:

$$(\Delta H_{1999})_{crist} = (\Delta H^0_{f,\,298})_{crist} + \int_{298}^{1999} (C_P)_{crist}\, dT$$

$$(\Delta H_{1999})^{liquid}_{SiO_2} = (\Delta H_{1999})_{crist} + (\Delta H_{fus})_{crist}$$

$$(\Delta H^0_{f,\,298})^{liquid}_{SiO_2} = (\Delta H_{1999})^{liquid}_{SiO_2} + \int_{1999}^{298} (C_P)_{SiO_2\,glass}\, dT.$$

The values calculated are then S^0_{298} (SiO$_2$ liquid) = 17.79 J/(mol·K) and ΔH^0_{298} (SiO$_2$ liquid) = -901.556 kJ/mol.

3. Activity coefficients (γ) for esseneite and calcium aluminum pyroxene were calculated as a function of composition and temperature, utilizing (1) experimental data for coexisting augite, feldspar, spinel, and glass (at a specific temperature and f_{O_2}); and (2) the regular solution model for silicate melts of Ghiorso et al. (1983). The reactions that we considered were CaAl$_2$SiO$_6$ + SiO$_2$ = CaAl$_2$Si$_2$O$_8$, where

$$\ln \gamma^{augite}_{CaAl_2SiO_6} = (G^0/RT + \ln a^{plagioclase}_{CaAl_2Si_2O_8} - \ln a^{liquid}_{SiO_2}$$
$$- \ln X^{augite}_{CaAl_2SiO_6})$$

and 3CaFe^{3+}AlSiO$_6$ + 1.5Al$_2$O$_3$ + 3SiO$_2$ = Fe$_3$O$_4$ + 3CaAl$_2$Si$_2$O$_8$ + 0.25O$_2$, where

$$\ln \gamma^{augite}_{CaFe^{3+}AlSiO_6} = (G^0/RT + 0.25 \ln f_{O_2} + 3 \ln a^{plagioclase}_{CaAl_2Si_2O_8}$$
$$+ \ln a^{spinel}_{Fe_3O_4} - \ln a^{liquid}_{SiO_2} - 1.5 \ln a^{liquid}_{Al_2O_3}$$
$$- 3 \ln X^{augite}_{CaFe^{3+}AlSiO_6})/3.$$

Free energy data given by Ghiorso et al. (1983), together with mineral and glass compositions reported from experiments by Mahood and Baker (1986), Sack et al. (1987), Tormey et al. (1987), Grove and Juster (1989), Grove et al. (1990), Kennedy et al. (1990), and Juster et al. (1990), have been used to derive γ for these two phases. Curves of X vs. $RT \ln \gamma$ can be fitted to the experimental data for each pyroxene component, thus allowing one to calculate γ as a function of pyroxene composition. The equations for these curves are esseneite: $RT \ln \gamma = (-9617.4 \ln X) - 4939.1$, and calcium aluminum pyroxene: $RT \ln \gamma = (-9715.6 \ln X) - 38002.0$, where X is the mole fraction of the pyroxene component according to Equation 2 in the text.